www.czasopisma.pan.pl PAN www.journals.pan.pl

ARCHIVES of FOUNDRY ENGINEERING

ISSN (2299-2944)
Volume 2023
Issue 3/2023

5 – 11

1/3

10.24425/afe.2023.144308

Published quarterly as the organ of the Foundry Commission of the Polish Academy of Sciences

Difficulties in the Production of Ausferritic Nodular Cast Iron without Heat Treatment

M. Stawarz [a, *], M. Lenert [a, b], K. Piasecki [a, b]

[a] Department of Foundry Engineering, Silesian University of Technology, Towarowa 7 St., 44-100 Gliwice, Poland

[b] Odlewnia RAFAMET Sp. z o.o., ul. Staszica 1, Kuźnia Raciborska, Poland

* Contact for correspondence: E-mail: marcin.stawarz@polsl.pl

Received 22.02.2023; accepted in revised form 03.06.2023; available online 24.07.2023

Abstract

The paper presents results of tests carried out on ausferrite carbide matrix alloyed ductile cast iron. The ausferrite was obtained via addition of Cu and Mo alloying elements. This eliminated heat treatment from the alloy production cycle. The article presents results of tests of the quality of the obtained material. Emphasis was put on metallographic analysis using light and scanning microscopy. Works also included chemical composition tests and EDS analysis. Strength tests were executed in an accredited laboratory. It is possible to create a raw ausferrite carbide matrix without subjecting an alloy to heat treatment. However, it turned out that quality parameters of cast iron were insufficient. The obtained material hardness was 515 HB, while Rm strength and A5 ductility were very low. The low tensile strength of the analyzed alloy resulted from the presence of degenerate graphite secretion (of flake or vermicular shape) in the cast iron. The tests also demonstrated that the alloy was prone to shrinkage-related porosity, which further weakened the material. Alloys made of alloyed ductile iron of ausferrite matrix micro-structure are very attractive due to elimination of the heat treatment process. However, their production process and chemical composition must be optimized.

Keywords: Ausferrite, Nodular cast iron, Alloyed cast iron, Casting quality, Vari-morph cast iron

1. Introduction

Ductile iron tempered using ADI isothermal process occurs in many varieties [1-3]. In the scientific literature, there are many works describing ductile iron [4-5], ductile iron for thin-walled alloys [6-7], as well as vermicular ductile iron [8] with an ausferrite matrix. The basis for production of such a ductile iron is heat treatment of alloys [9-10]. As a result of heat treatment, cast iron obtains unique use properties. It increases the tensile strength and hardness [11], as well as allows maintaining a certain limit of plasticity. As a result, ADI ductile iron may be used in many industrial solutions, which take advantage of its unique characteristics, such as its resistance to abrasion wear [12-14]. However, this material also has flaws. The main one is a limited alloy use temperature, which is below isothermal tempering temperature. Another problem is expensive heat treatment, which is long and requires costly devices. It also consumes a lot of energy. Moreover, quenching tanks are filled with salts that cause surface corrosion on alloys. Salt baths used for ductile iron isothermal tempering are harmful for the environment. Due to use of austenitization furnaces and tempering tanks, the size of alloys, in which we may create the ausferrite micro-structure, is limited.

The literature provides methods of elimination of heat treatment from the process of ADI ductile iron production [15]. It is possible to directly cool ductile iron [16] or use alloying elements [17-22] that ensure obtaining of an ausferrite micro-structure. This is a very attractive solution, in particular considering the rapidly growing energy prices.

The aim of the work is initially to identify the possibility of producing large-sized castings with an ausferrite matrix. The planned effect of the work is the recognition of errors (on a laboratory scale) that may accompany the production of castings on a macroscale weighing more than 1000 kg with an ausferritic matrix, without heat treatment.

2. Materials and Methods

Experimental melting was carried out in an induction furnace of medium frequency and capacity of 25 kg. Circulating scrap of chemical composition presented in Table 1, item A, was used as input material. During the experimental melting, the chemical composition of the cast iron was supplemented with Mo alloying additions in a form of FeMo65 and Cu in its pure form Cu99.9E. After overheating the metal bath to 1530°C, we collected a sample for the chemical composition analysis (Tab. 1, item B). The alloy temperature was lowered to 1420°C; then, we carried out balling using the flexible cable method and Cedifil NCD 4800 flux-cored wire. Next, we applied Inoculin 400 modifier on the metal stream. A cylinder of Ø30 mm and 50 cm height (alloy mold 0.74 cm) was cast and a sample for chemical composition analysis was collected (Tab. 1, item C). The chemical composition analysis was performed using Leco GDS500A spark spectrometer. Metallographic tests were executed using Nicon Eclipse LV500N light microscope and Nikon NIS-Element F 3.00 software, as well as Phenom ProX scanning microscope with EDS system. Strength tests were carried out using Louis Schopper Staatl static strength test machine and Falcon 500G2 hardness tester. Metallographic tests were performed on samples etched in 3% Nital solution in bright field and dark field using filters available in Nikon NIS-Element F 3.00 software and in fresh fractures.

Table 1.
Chemical composition of cast iron

	Chemical composition, wt. %								
	C	Si	Mo	Cu	Mn	P	S	Mg	Fe
A	3.92	2.20	0	0.04	0.71	0.04	0.012	0	bal.
B	3.65	2.01	2.03	1.99	0.64	0.04	0.027	0	bal.
C	3.60	2.51	2.07	1.96	0.65	0.03	0.024	0.07	bal.

A - *iron scrap*, B - *preliminary cast iron before spheroidization treatment*,
C - *final cast iron after spheroidization treatment*

3. Research results and discussion

3.1. Light microscopy

Figures 1-8 present the micro-structures of obtained cast iron. In the micro-structures, there are visible graphite precipitates in the ausferrite matrix. Furthermore, on the borders of grains there are bright precipitates of molybdenum carbide Mo_2C. All identified elements of the micro-structure are marked and described in the photos below.

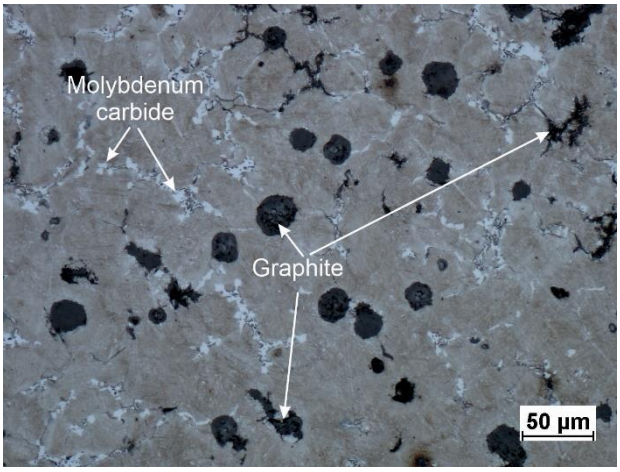

Fig. 1. Ausferrite microstructure with nodular graphite and molybdenum carbide for casting No. C, etched 3% Nital

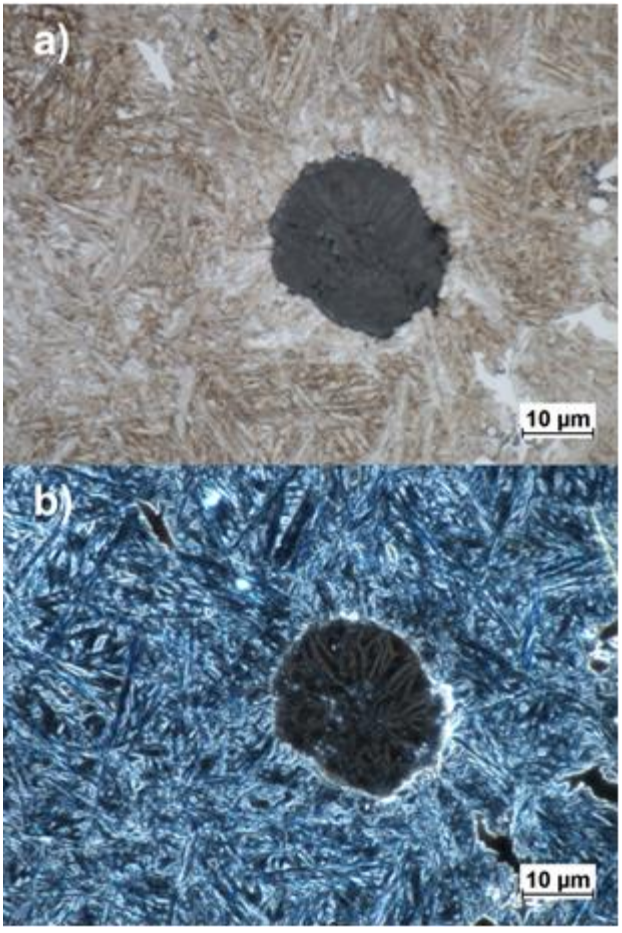

Fig. 2. Ausferrite microstructure with nodular graphite for casting No. C, etched 3% Nital, a - bright field, b – dark field

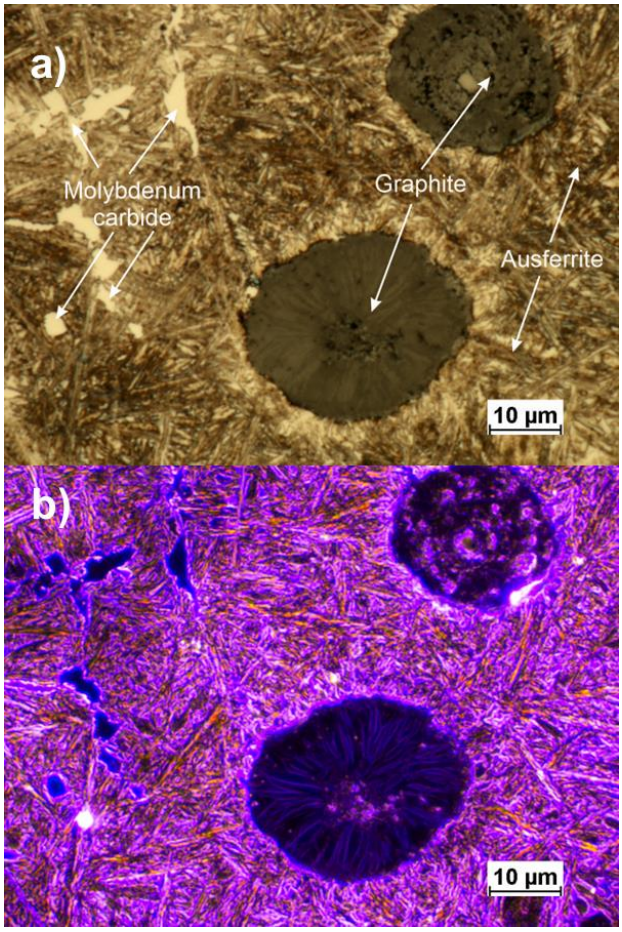

Fig. 3. Ausferrite microstructure with nodular graphite and molybdenum carbide for casting No. C, etched 3% Nital, a - bright field, b – dark field

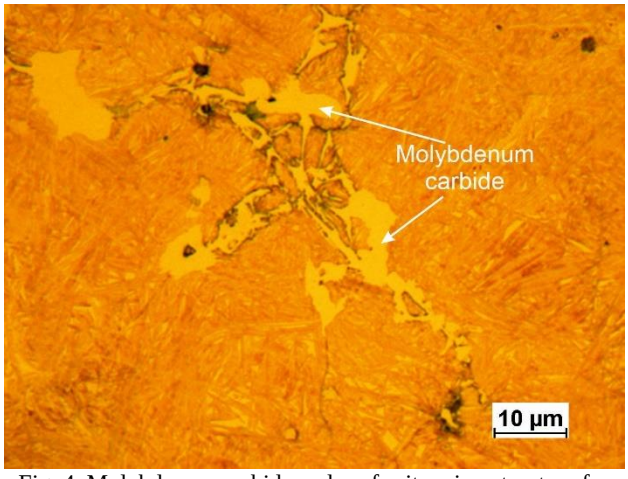

Fig. 4. Molybdenum carbide and ausferrite microstructure for casting No. C, etched 3% Nital

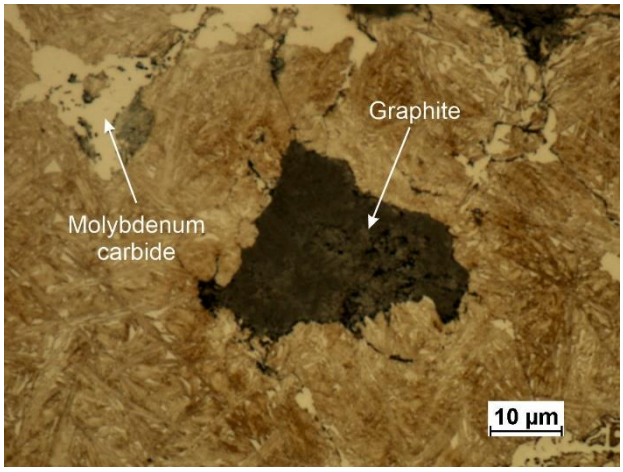

Fig. 5. Ausferrite microstructure with degenerate nodular graphite and molybdenum carbide for casting No. C, etched 3% Nital

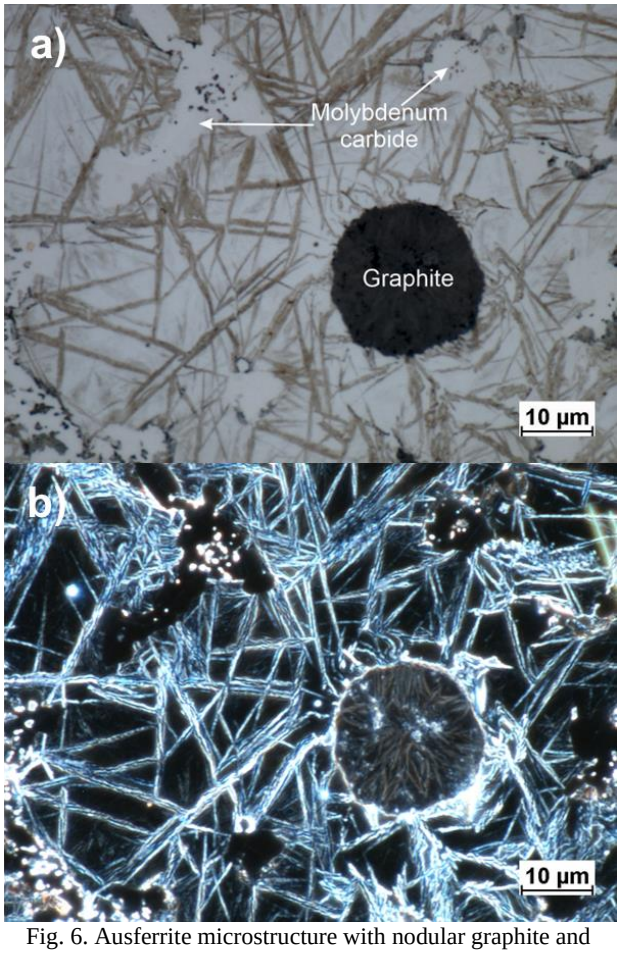

Fig. 6. Ausferrite microstructure with nodular graphite and molybdenum carbide for casting No. C, etched 3% Nital, a - bright field, b – dark field. Half-etched sample

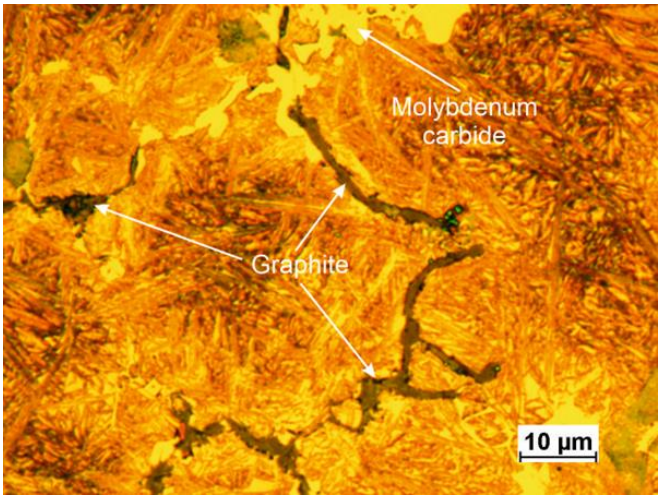

Fig. 7. Flake graphite participations and molybdenum carbide with ausferrite matrix for casting No. C, etched 3% Nital

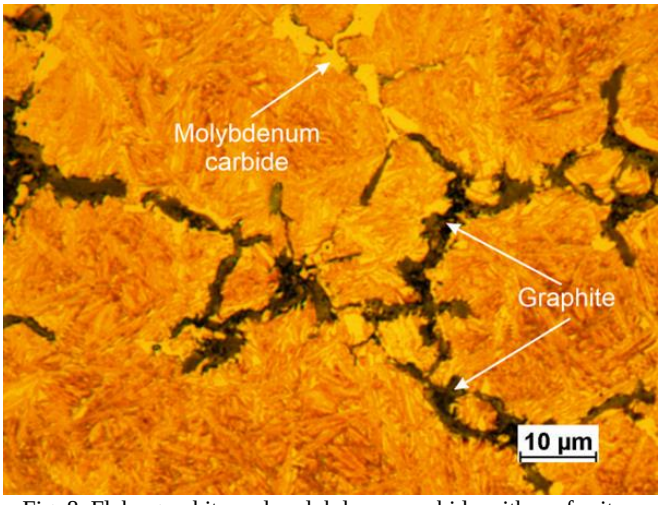

Fig. 8. Flake graphite and molybdenum carbide with ausferrite matrix for casting No. C, etched 3% Nital

As you can see, in the presented micro-structures of the obtained alloy, we may identify highly degenerated spheroidal graphite precipitates (Fig. 5) and flake graphite precipitates (Fig. 7-8). This is caused by the impact of alloying elements on the graphite crystallization process. Papers [23-24] mention the phenomenon of degeneration of spheroidal graphite to the flake form in case of alloys of increased Mo content. The correct process of spheroidal graphite crystallization is also impacted by high level of Cu. As shown in papers [25-28], Cu negatively impacts the process of spheroidal graphite crystallization, whereas different authors indicate various limit values of participation of copper, above which graphite is subject to degradation.

3.2. SEM and EDS analysis

In order to carry out more detailed assessment of the quality of the analyzed alloy, scanning microscopy was used.

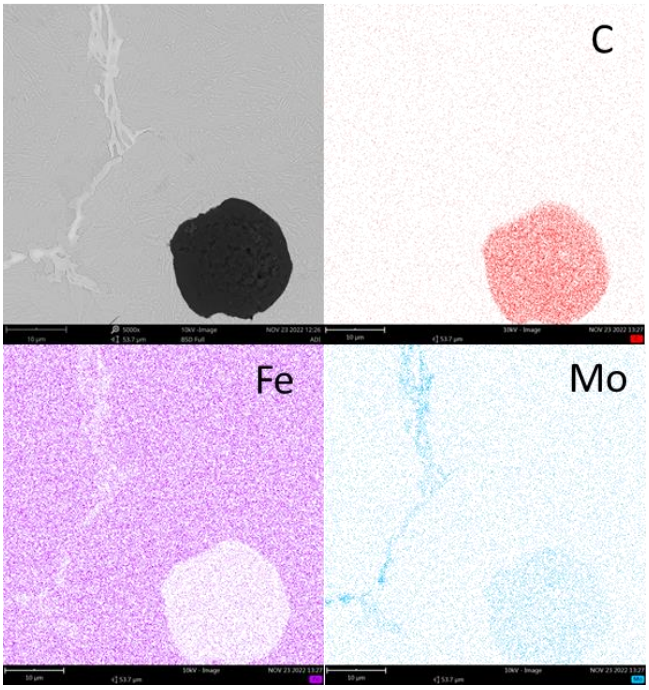

Fig. 9. The analysis of a EDS for nodular graphite and molybdenum carbide

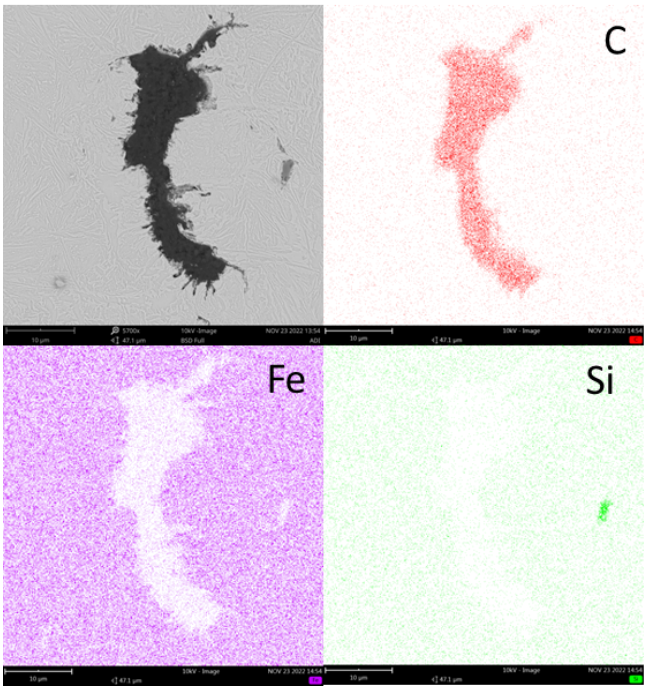

Fig. 10. The analysis of a EDS for degenerate graphite

The EDS analysis results presented in photo 9 confirm that bright precipitates on the borders of grains contain high amounts of molybdenum. Therefore, in case of the system of elements typical for the analyzed alloy, we are dealing with molybdenum carbides Mo_2C. This is also confirmed by other papers [29-30].

The chemical composition of the degenerated spheroidal graphite precipitates was also confirmed. Photo 10 shows a vermicular secretion, which clearly contains a lot of carbon. Such a result unambiguously identifies it as a graphite secretion.

The next stage of SEM analysis included analyzes carried out on the fractures of the tested alloy. The results of those analyzes are presented in photos 11-13.

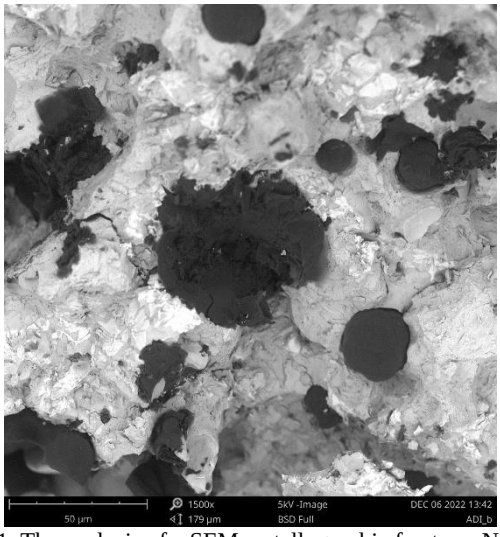

Fig. 11. The analysis of a SEM metallographic fracture. Nodular and degenerate graphite

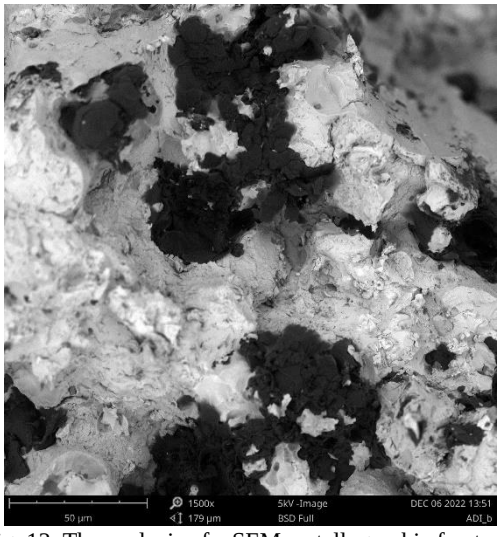

Fig. 12. The analysis of a SEM metallographic fracture. Degenerate nodular graphite

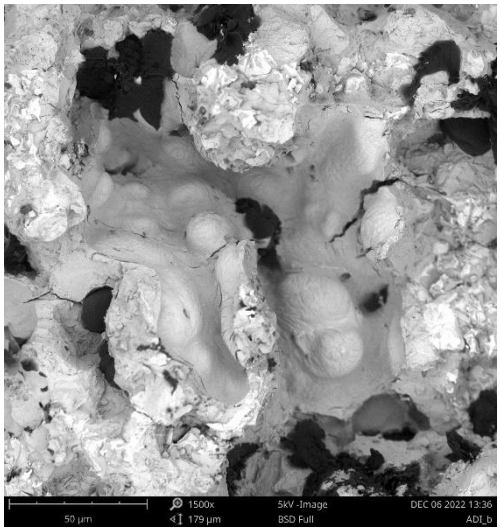

Fig. 13. The analysis of a SEM metallographic fracture. Shrinkage cavity. Nodular and degenerate graphite

As shown in photos 11-13, the graphite precipitates disclosed at the fractures are significantly degenerated. The additional lack of continuity of the matrix, which decreases the quality of the alloy, is shown in photo 13. Here, we can see shrinkage. If such defects are present in case of 0.74 cm alloy mold, we may expect an accumulation of such defects in case of alloys of larger dimensions.

3.3. Mechanical properties testing

The last stage of tests included strength tests based on the obtained material. Due to the specificity of the presented experiment (initial tests), a Y type sample was not cast – only an Ø30 mm cylinder was cast. From this cylinder, a sample of dimensions in line with PN EN 1564 was machined. The obtained results are presented in Table 2.

Table 2.
Mechanical properties of alloyed cast iron No. C

	Rm, MPa	A5, %	HB
C	223	0.8	515

Based on the obtained strength tests, it may be stated that the value of hardness is significantly higher than the values for ADI cast iron included in standard 1564. This results mainly from the presence of molybdenum carbide in the matrix, which increases this value. The tensile strength is low due to lack of homogeneity of the graphite precipitates (there are vermicular graphite precipitates and flake graphite present near the spheroidal graphite), which decreases the Rm value. Moreover, the shrinkages identified in the analyzed alloy significantly reduce the Rm value of the tested alloy.

4. Conclusions

The conclusions drawn from the performed tests were as follows:

- Cast iron with a correct matrix micro-structure (ausferrite) was successfully obtained without heat treatment.
- Due to the high content of alloying additives (Cu and Mo), the tensile strength is significantly lower. The reason for that is degeneration of certain graphite precipitates from spherical to vermicular or flake shape.
- The described material shows tendency for shrinkage-related porosity, which negatively impacts its tensile strength.
- The value of the obtained hardness of the analyzed samples is very high due to presence of molybdenum carbide on the borders of grains.
- The obtained cast iron may be qualified as vari-morph [31] cast iron with carbides.

Acknowledgements

The tests were financed by the Ministry of Science and Higher Education as a part of the 4th edition of "Doktoraty Wdrożeniowe" program carried out by the Faculty of Mechanical Engineering of the Silesian University of Technology.

References

[1] Ahmed, M., Riedel, E., Kovalko, M., Volochko, A., Bähr, R. & Nofal, A. (2022). Ultrafine ductile and austempered ductile irons by solidification in ultrasonic field. *International Journal of Metalcasting.* 16(3), 1463-1477. DOI:10.1007/s40962-021-00683-8.

[2] Benam, A.S. (2015). Effect of alloying elements on austempered ductile iron (ADI) properties and its process: review. *China Foundry*. 12(1), 54-70.

[3] Uyar, A., Sahin, O., Nalcaci, B., & Kilicli. V. (2022). Effect of austempering times on the microstructures and mechanical properties of dual-matrix structure austempered ductile iron (DMS-ADI). *International Journal of Metalcasting*. 16(1), 407-418. DOI:10.1007/s40962-021-00617-4.

[4] Lefevre, J. & Hayrynen. K.L. (2013). Austempered materials for powertrain applications. *Journal of Materials Engineering and Performance*. 22(7), 1914-1922. DOI:10.1007/s11665-013-0557-4.

[5] Tyrała, E., Górny, M., Kawalec, M., Muszyńska, A. & Lopez, H.F. (2019). Evaluation of volume fraction of austenite in austempering process of austempered ductile iron. *Metals*. 9(8), 1-10. DOI:10.3390/met9080893.

[6] Fraś, E., Górny, M., Tyrała, E. & Lopez. H. (2012). Effect of nodule count on austenitising and austempering kinetics of ductile iron castings and mechanical properties of thin walled iron castings. *Materials Science and Technology*. 28(12), 1391-1396. DOI:10.1179/1743284712Y.0000000088.

[7] Ibrahim, M.M., Negm, A.M., Mohamed, S.S. & Ibrahim. K.M. (2022). Fatigue properties and simulation of thin wall ADI and IADI castings. *International Journal of Metalcasting*. 16(4), 1693-1708. DOI:10.1007/s40962-021-00711-7.

[8] Gumienny, G. & Kacprzyk. B. (2018). Copper in ausferritic compacted graphite iron. *Archives of Foundry Engineering*. 18(1), 162-166. DOI:10.24425/118831.

[9] Abdullah, B., Alias, S. K., Jaffar, A., Rashid, A.A., Ramli, A. (2010). Mechanical properties and microstructure analysis of 0.5% niobium alloyed ductile iron under austempered process in salt bath treatment. International Conference on Mechanical and Electrical Technology, (pp. 610-614). DOI:10.1109/ICMET.2010.5598431.

[10] Akinribide, O.J., Ogundare, O.D., Oluwafemi, O.M., Ebisike, K., Nageri, A.K., Akinwamide, S.O., Gamaoun, F. & Olubambi, P.A. (2022). A review on heat treatment of cast iron: phase evolution and mechanical characterization. *Materials*. 15(20), 1-38. DOI:10.3390/ma15207109.

[11] Samaddar, S., Das, T., Chowdhury, A.K., & Singh, M. (2018). Manufacturing of engineering components with Austempered ductile iron - A review. *Materials Today: Proceedings*. 5(11), 2561525624. DOI:10.1016/j.matpr. 2018.11.001.

[12] Stachowiak, A., Wieczorek, A.N., Nuckowski, P., Staszuk, M. & Kowalski, M. (2022). Effect of spheroidal ausferritic cast iron structure on tribocorrosion resistance. *Tribology International*. 173. DOI:10.1016/j.triboint.2022.107688.

[13] Myszka, D. & Wieczorek, A. (2015). Effect of phenomena accompanying wear in dry corundum abrasive on the properties and microstructure of austempered ductile iron with different chemical composition. *Archives of Metallurgy and Materials*. 60(1), 483-490. DOI:10.1515/amm-2015-0078.

[14] Pimentel, A.S.O., Guesser, W.L., Portella, P.D., Woydt, M. & Burbank. J. (2019). Slip-rolling behavior of ductile and austempered ductile iron containing niobium or chromium. *Materials Performance and Characterization*. 8(1), 402-418. DOI:10.1520/MPC20180188.

[15] Machado, H.D., Aristizabal-Sierra, R., Garcia-Mateo, C. & Toda-Caraballo, I. (2020). Effect of the starting microstructure in the formation of austenite at the intercritical range in ductile iron alloyed with nickel and copper. *International Journal of Metalcasting*. 14(3), 836-845. DOI:10.1007/s40962-020-00450-1.

[16] Janowak, J.F. & Gundlach. R.B. (1985). Approaching austempered ductile iron properties by controlled cooling in the foundry. *Journal of Heat Treating*. 4(1), 25-31. DOI:10.1007/BF02835486.

[17] Gumienny, G. & Kurowska, B. (2018). Alternative technology of obtaining ausferrite in the matrix of spheroidal cast iron. *Transactions of the Foundry Research Institute*. 58(1), 13-29. DOI: 10.7356/iod.2018.02.

[18] Gumienny, G., Kacprzyk, B., Mrzygłód, B. & Regulski. K. (2022). Data-driven model selection for compacted graphite iron microstructure prediction. *Coatings*. 12(11). DOI:10.3390/coatings12111676.

[19] Tenaglia, N.E., Pedro, D.I., Boeri, R.E. & Basso. A.D. (2020). Influence of silicon content on mechanical properties of IADI obtained from as cast microstructures. *International Journal of Cast Metals Research*. 33(2-3), 72-79. DOI:10.1080/13640461.2020.1756082.

[20] Méndez, S., De La Torre, U., González-Martínez, R. & Súarez. R. (2017). Advanced properties of ausferritic ductile iron obtained in as-cast conditions. *International Journal of Metalcasting*. 11(1), 116-122. DOI:10.1007/s40962-016-0092-9.
[21] Kashani, S.M. & Boutorabi. S. (2009). As-cast acicular ductile aluminum cast iron. *Journal of Iron and Steel Research International*. 16(6), 23-28. DOI:10.1016/S1006-706X(10)60022-2.
[22] Ferry, M. & Xu. W. (2004). Microstructural and crystallographic features of ausferrite in as-cast gray iron. *Materials Characterization*. 53(1), 43-49. DOI:10.1016/j.matchar.2004.07.008.
[23] Stawarz, M. & Nuckowski. P. M. (2022). Corrosion behavior of simo cast iron under controlled conditions. *Materials*. 15(9), 1-14. DOI:10.3390/ma15093225.
[24] Stawarz, M. (2018). Crystallization process of silicon molybdenum cast iron. *Archives of Foundry Engineering*. 18(2), 100-104. DOI:10.24425/122509.
[25] Vaško, A., Belan, J. & Tillová. E. (2018). Effect of copper and molybdenum on microstructure and fatigue properties of nodular cast irons. *Manufacturing Technology*. 18(6), 1049-1052. DOI:10.21062/ujep/222.2018/a/1213-2489/mt/18/6/1048.
[26] Silman, G.I., Kamynin, V.V. & Tarasov. A.A. (2003). Effect of copper on structure formation in cast iron. *Metal Science and Heat Treatment*. 45(7-8), 254-258. DOI:10.1023/A:1027320116132.
[27] Gumienny, G., Kacprzyk, B. & Gawroński, J. (2017). Effect of copper on the crystallization process, microstructure and selected properties of CGI. *Archives of Foundry Engineering*. 17(1), 51-56. DOI:10.1515/afe-2017-0010.
[28] Vaško, A. (2017). Fatigue properties of nodular cast iron at low frequency cyclic loading. *Archives of Metallurgy and Materials*. 62(4), 2205-2210. DOI:10.1515/amm-2017-0325.
[29] Stawarz, M. & Nuckowski. P.M. (2020). Effect of Mo addition on the chemical corrosion process of SiMo cast iron. *Materials*. 13(7), 1-10. DOI:10.3390/ma13071745.
[30] Stawarz, M. (2017). SiMo ductile iron crystallization process. *Archives of Foundry Engineering*. 17(1), 147-152. DOI:10.1515/afe-2017-0027.
[31] Zych, J., Myszka, M. & Kaźnica, N. (2019). Control of selected properties of „Vari-morph" (VM) cast iron by means of the graphite form influence, described by the mean shape indicator. *Archives of Foundry Engineering*. 19(3), 43-48. DOI:10.24425/afe.2019.127137.